Title

Structurally plastic NEMO and oligomerization prone IKK2 subunits define the behavior of human IKK2:NEMO complexes in solution

Journal

Biochimica et Biophysica Acta (BBA) - Proteins and Proteomics, 1868(12)

ISSN

1570-9639

Authors

Ko, Myung Soo
Biswas, Tapan
Mulero, Maria Carmen
et al.

Publication Date

2020-12-01

DOI

10.1016/j.bbapap.2020.140526

Peer reviewed

HHS Public Access

Author manuscript

Biochim Biophys Acta Proteins Proteom. Author manuscript; available in PMC 2021 March 25.

Published in final edited form as:

Biochim Biophys Acta Proteins Proteom. 2020 December ; 1868(12): 140526. doi:10.1016/j.bbapap.2020.140526.

Structurally plastic NEMO and oligomerization prone IKK2 subunits define the behavior of human IKK2:NEMO complexes in solution

Myung Soo Ko[a,b], **Tapan Biswas**[b], **Maria Carmen Mulero**[c], **Andrey A. Bobkov**[d], **Gourisankar Ghosh**[b,*], **Tom Huxford**[a,*]

[a]Structural Biochemistry Laboratory, Department of Chemistry & Biochemistry, San Diego State University, 5500 Campanile Drive, San Diego, CA 92182-1030, United States

[b]Department of Chemistry & Biochemistry, University of California, San Diego, 9500 Gilman Drive, La Jolla, CA 92093-0357, United States

[c]UC San Diego Moores Cancer Center, United States

[d]Sanford Burnham Prebys Medical Discovery Institute, United States

Abstract

The human IκB Kinase (IKK) is a multisubunit protein complex of two kinases and one scaffolding subunit that controls induction of transcription factor NF-κB activity. IKK behaves as an entity of aberrantly high apparent molecular weight in solution. Recent X-ray crystallographic and cryo-electron microscopy structures of individual catalytic subunits (IKK1/IKKα and IKK2/IKKβ) reveal that they are both stably folded dimeric proteins that engage in extensive homo-oligomerization through unique surfaces that are required for activation of their respective catalytic activities. The NEMO/IKKγ subunit is a predominantly coiled coil protein that is required for activation of IKK through the canonical NF-κB signaling pathway. Here we report size-exclusion chromatography, multi-angle light scattering, analytical centrifugation, and thermal denaturation analyses of full-length human recombinant NEMO as well as deletion and disease-linked variants. We observe that NEMO is predominantly a dimer in solution, although by virtue of its modular coiled coil regions NEMO exhibits complicated solution dynamics involving portions that are mutually antagonistic toward homodimerization. This behavior causes NEMO to behave as a significantly larger sized particle in solution. Analyses of NEMO in complex with IKK2 indicate that NEMO preserves this structurally dynamic character within the multisubuit complex and provides the complex-bound IKK2 further propensity toward homo-oligomerization. These observations provide critical information on the structural plasticity of NEMO subunit dimers which helps clarify its role in diseases and in IKK regulation through oligomerization-dependent phosphorylation of catalytic IKK2 subunit dimers.

*Corresponding authors: gghosh@ucsd.edu (G. Ghosh), thuxford@sdsu.edu (T. Huxford).

Declaration of Competing Interest

The authors declare that they have no known competing financial interests or personal relationships that could have appeared to influence the work reported in this paper.

Appendix A. Supplementary data

Supplementary data to this article can be found online at https://doi.org/10.1016/j.bbapap.2020.140526.

Keywords

Analytical ultracentrifugation; Circular dichroism spectroscopy; IκB kinase; Multi-angle light scattering; NEMO; NF-κB; Size-exclusion chromatography

1. Introduction

Induction of transcription factor NF-κB in response to diverse environmental challenges and intracellular stresses requires activation of the IκB Kinase (IKK) [1,2]. Human IKK is a multisubunit complex that consists of two highly similar kinase domain-containing proteins known as IKK1/IKKα and IKK2/IKKβ as well as a necessary scaffolding subunit referred to as NF-κB Essential Modulator or NEMO/IKKγ (hereafter referred to as IKK1, IKK2, and NEMO, respectively) [3,4]. IKK was discovered biochemically as the only cellular activity in TNF-α-induced HeLa cell cytoplasmic extracts that could selectively phosphorylate the NF-κB inhibitor protein IkBα at serines 32 and 36 [5–7]. Early characterization of active IKK via size-exclusion chromatography (SEC) revealed that it behaves in solution as a 700–900 κDa complex [6–8]. While this suggests the presence of multiple copies of IKK1 (85 kDa), IKK2 (87 kDa), and/or NEMO (48 kDa), the precise number and arrangement of individual subunits in the functional IKK complex has been a matter of debate. Furthermore, the molecular mechanism by which IKK becomes active in response to a plethora of distinct cellular stimuli has also remained unclear. Detailed knowledge of the IKK activation mechanism to a level that can guide discovery of novel targeted therapeutic strategies requires a clearer understanding of the assembly and solution dynamics of IKK subunits.

Independent structural models for IKK1 and IKK2 subunits as well as analyses of their respective behavior in solution have emerged from experimental biophysical studies on purified, individual IKK subunit proteins. The X-ray crystal structure of nearly full-length IKK2 revealed it to be a stably folded homodimer [9–11]. IKK2 dimerization is mediated by interaction through its C-terminal scaffold dimerization domain (SDD) that exhibits hinge-like properties and, consequently, supports considerable variation in the distance between N-terminal kinase domains (KD) of IKK2 homodimers. Engineered deletion of the distal portion of the SDD that mediates dimerization resulted in a stable monomeric version of IKK2 that preserves its structure and catalytic specificity toward the IκBα substrate protein [12]. Interestingly, IKK2 dimers demonstrate a propensity toward higher order oligomerization in solution. Structure-based scanning mutagenesis of residues from different areas on the surface of the KD that stabilize the “open” conformation of IKK2 homodimers observed in some crystal structures implicated these surfaces as necessary for converting inactive IKK to its active state [10]. The hallmark of active IKK in response to canonical NF-κB signaling is the phosphorylation of serines 177 and 181, within the activation segment of the IKK2 subunit kinase domain [13]. As with many protein kinases, phosphorylation within this region serves to arrange active site residues so that they are capable of supporting transfer of the gamma-phosphate from ATP to substrate proteins [14]. Structural studies of IKK1 revealed that it adopts a similar homodimeric structure to IKK2 and also tends toward self-association in solution [15]. However, IKK1 oligomerization involves unique amino acid residues that map to different surfaces than those required for

IKK2 self-association. Alteration of these residues was sufficient to disrupt key steps in alternative NF-κB signaling, which is mediated through the catalytic activity of IKK1 [15–17].

NEMO is an integral component of multisubunit IKK complexes that is required for canonical NF-κB signaling through IKK2 [18,19]. The precise mechanism by which NEMO serves to integrate diverse signaling inputs to yield phosphorylation-dependent activation of IKK2 remains unknown. However, it is clear that inducible formation of polyubiquitin chains plays a vital upstream role in this process [20].

NEMO was predicted from its amino acid sequence to be a primarily coiled coil (CC) protein with a zinc finger domain at its extreme C-terminus [3,21]. Although no structure for the full-length protein is known, X-ray crystal structures of several segments conform with this prediction. An N-terminal region spanning residues 49–109 in human NEMO has been shown to mediate the principal interaction with the C-terminal NEMO binding domain (NBD) in catalytic IKK2 and IKK1 subunits [22,23]. X-ray crystal structures of this kinase binding domain (KBD) portion in NEMO in complex with residues 705–743 from the C-terminus of IKK2 and in its free form revealed the KBD to be a dynamic CC homodimer that can open slightly to accommodate binding of the catalytic subunit [24,25]. Three-dimensional structures of several other segments of NEMO include the vFLIP binding CC1 spanning residues 192 to 252 [26], the CC2 at residues 263–333 (also commonly referred to as CoZi or UBAN) that binds to linear diubiquitin and the HOIP linear ubiquitin assembly complex (LUBAC) subunit NZF1 domain [27–30], a Pro-rich segment (residues 388–393) that binds the CYLD deubiquitinase (DUB) [31], and ubiquitin-binding C-terminal Zn finger domain (residues 394–419) [32].

NEMO is encoded by an X-linked gene and NEMO dysfunction due to point mutations or deletions is often associated with the inherited diseases incontinentia pigmenti (IP) and ectodermal dysplasia anhidrotic with immunodeficiency (EDA-ID) [33]. The severity of EDA-ID and IP is highly variable among patients and depends upon the specific NEMO mutation. Whereas functional defects arising from some mutations can be readily explained, such as disruption of ubiquitin chain binding or NEMO ubiquitylation, the mechanisms through which many NEMO mutations confer disease phenotypes are not known.

Despite the direct observation of multiple homodimeric CC regions, the structure and oligomerization state of full-length human NEMO in solution remains a point for discussion. Early attempts at studying NEMO oligomerization via diverse methods including chemical cross-linking, sedimentation, and chromatography suggested various oligomeric states for NEMO in solution including monomer, dimer, trimer, and tetramer [21,34–36]. The lack of clarity surrounding the solution behavior of NEMO is exacerbated by the aforementioned observation that multisubunit IKK complexes are routinely purified from cells with an apparent mass of 700–900 kDa [6–8,10].

In this study we used current structural understanding of individual IKK subunit proteins to engineer human NEMO as a recombinant full-length protein, as various deletion constructs, and as variants containing disease-linked point mutations. Purified NEMO protein constructs

both independently and in complex with recombinant IKK2 subunit homodimers were subjected to experimental biophysical approaches to characterize their oligomerization state and solution behavior. Size-exclusion chromatography coupled with multi-angle light scattering (SEC-MALS) and analytical ultracentrifugation (AUC) measurements clearly indicate that full-length human NEMO assembles predominantly as a homodimer. Some, but not all, of the truncated fragments and many disease-linked NEMO variants harboring point mutations exhibit defects in dimerization. In association with IKK2, the resulting IKK2:NEMO complexes form homodimer:homodimer tetramers that exhibit an even greater tendency toward higher order oligomerization than has been observed previously with human IKK2 homodimers alone. The NEMO deletion constructs and variants containing disease-linked point mutations studied here assemble with IKK2 in a manner similar to the full-length NEMO.

2. Materials and methods

2.1. Recombinant plasmid and baculovirus preparation

Full-length human NEMO (Uniprot Accession ID: Q9Y6K9) and deletion constructs ($NEMO^{1–110}$, $NEMO^{1–130}$, $NEMO^{1–210}$, $NEMO^{1–250}$, $NEMO^{1–280}$, $NEMO^{1–365}$, $NEMO^{111–250}$, and $NEMO^{250–365}$) were subcloned individually into the *Nde*I and BamHI restriction sites of the pET15b vector in frame with an N-terminal hexahistidine tag. For site-directed mutagenesis, all substitutions of seven mutations causing EDAID in males and three that cause IP in females mapped within the IVD and CC1 regions (110–250) were generated within the pET15b plasmid harboring wild-type NEMO. Ten single amino acid substitutions, $NEMO^{D113N}$, $NEMO^{R123W}$, $NEMO^{V146G}$, $NEMO^{L153R}$, $NEMO^{Q157P}$, $NEMO^{A162P}$, $NEMO^{R173G}$, $NEMO^{R173Q}$, $NEMO^{R175P}$, and $NEMO^{L227P}$, were prepared by PCR with base changes incorporated in the oligonucleotide primers. Human IKK2 cDNA (Uniprot Accession ID: O14920) was graciously provided by the laboratory of M. Karin (School of Medicine, UC, San Diego). Full-length IKK2 (amino acids 1–756) was amplified by PCR and cloned in pFastBacHTb (Invitrogen) vector within BamHI and *Not*I sites in frame with an N-terminal hexahistidine-TEV cleavage site tag. Recombinant baculovirus production, amplification, and titer optimization were carried out in Sf9 insect cell suspensions as described previously [37].

2.2. Protein expression and purification

All His-tagged NEMO proteins were expressed in BL21 (DE3) cells. 1 L cultures in LB media with 100 μg/mL ampicillin were grown at 37 °C to OD600 of 0.2 before induction with 0.2 mM isopropyl β-D-1-thiogalactopyranoside (IPTG) (Biobharati) and stirring at 150 rpm for 22 °C for 16 h. Cells were harvested by centrifugation at 3000 ×*g* for 10 min (Beckman Coulter) and cell pellets were lysed by sonication (VWR Scientific) on ice in 200 mL of lysis buffer (20 mM Tris-HCl pH 8.0, 300 mM NaCl, 10% *w/v* glycerol, 10 mM imidazole, 0.2% Triton X-100, 1 mM PMSF, and 5 mM β-mercaptoethanol). Lysates were clarified by centrifugation at 15,000 rpm for 45 min. Supernatants containing soluble proteins were then applied to a 1 mL Ni NTA-Agarose (Biobharati) column that was preequilibrated with lysis buffer. Bound proteins were washed with 25 mL wash buffer (lysis buffer with 30 mM imidazole) and eluted in 10 mL elution buffer (lysis buffer containing

250 mM imidazole). Sf9 insect cells from 1 L suspension cultures were harvested by centrifugation at 3000 ×*g* for 10 min at 4 °C and lysed by sonication in 100 mL of lysis buffer (25 mM Tris-HCl, pH 8.0, 200 mM NaCl, 10 mM imidazole, 10% *w/v* glycerol, 5 mM β-mercaptoethanol). The lysate was clarified by centrifugation at 18,000 rpm for 45 min at 4 °C. Pre-equilibrated Ni NTA-Agarose resin was added at a ratio of 1 mL of resin slurry/l of lysed cell culture and the mixture was incubated on a rotator at 4 °C for 3 h. The Ni beads were pelleted at 1000 rpm for 2 min in a swinging bucket centrifuge rotor. Supernatant was carefully decanted and the protein-bound resin was resuspended with wash buffer (lysis buffer containing 30 mM imidazole) and incubated at 4 °C on a rotator for 2 min. The Ni beads were pelleted again and decanted (wash 1). This was repeated until the last wash fraction contained 0.01–0.1 mg/mL of protein (Bio-Rad Protein Assay). Elution buffer (lysis buffer containing 250 mM imidazole) was added, and eluted fractions were collected and stored in −80 °C.

2.3 Size-exclusion chromatography

To investigate the degree of self-association, all purified individual NEMO and IKK2 proteins as well as NEMO:IKK2 complexes were subjected to gel filtration with a Superose6 Increase10/300 GL size-exclusion column (GE Healthcare) on an NGC™ Liquid Chromatography System (Bio-Rad). In general, equimolar concentrations of recombinant IKK2 and NEMO proteins were used during complex formation. NEMO:IKK2 complexes prepared at 2:1 molar excess of either subunit were indistinguishable from complexes purified after combining equimolar amounts. The column was equilibrated in a buffer with 25 mM Tris-HCl, pH 8.0, 250 mM NaCl, 2 mM DTT, and 5% glycerol at a flow rate of 0.2 mL/min at 22 °C. Molecular weight standards used are as follows: thyroglobulin, 670 kDa; gamma-globulin, 158 kDa; ovalbumin, 44 kDa; myoglobin, 17 kDa; vitamin B12, 1.4 kDa (Bio-Rad). The calibration standard data fit to the function:

$$\text{Apparent Molecular Weight}(V_E) = 0.0101\,V_E^2 + 00307\,V_E + 3.6298$$

where V_E is the measured elution volume of the protein. Peak fractions were analyzed by SDS-PAGE.

2.4. Size-exclusion chromatography-multi-angle light scattering analysis

Size-exclusion chromatography coupled multi-angle light scattering (SEC-MALS) was performed on an Agilent Technologies 1200 Series HPLC chromatography system equipped with a miniDAWN TREOS MALS detector and an Optilab TrEX differential refractive index detectors (Wyatt Technology). The SEC-MALS system was calibrated with bovine serum album. An aliquot of 100 μL of each sample was centrifuge-filtered prior to being loaded onto a Superose6 increase10/300 GL size-exclusion column (GE Life Science) and eluted in a buffer containing 25 mM Tris-HCl, pH 8.0, 250 mM NaCl, 2 mM DTT, and 5% glycerol at a flow rate of 0.4 mL/min at 22 °C. Absorbance was measured at 280 nm, and the MW was determined from the Raleigh ratio calculated by measuring the static light scattering and corresponding protein concentration of a selected peak using ASTRA VI software (Wyatt Technology).

2.5. Analytical ultracentrifugation analysis

Sedimentation velocity experiments were performed in a ProteomeLab XL-I (Beckman Coulter) analytical ultracentrifuge. NEMO and NEMO:IKK2 complex were purified and prepared as previously described. Protein samples at a concentration of 0.4 mg/mL in SEC buffer containing 1 mM TCEP were loaded in two-channel cells and spun in an An-50 Ti 8-place rotor at 30,000 rpm at 21 °C for 16 h. Absorbance at 280 nm was used for detection. Sedimentation velocity data were analyzed using Sedfit software [38].

2.6. Thermal stability analysis

Thermal melting experiments of NEMO and deletion constructs ($NEMO^{1–110}$, $NEMO^{1–130}$, $NEMO^{1–210}$, $NEMO^{1–250}$, $NEMO^{1–365}$, $NEMO^{250–365}$, $NEMO^{250–419}$ and single point mutation variants $NEMO^{D113N}$, $NEMO^{V146G}$, $NEMO^{L153R}$, $NEMO^{Q157P}$, $NEMO^{A162P}$, $NEMO^{R173G}$, $NEMO^{R173Q}$, $NEMO^{R175P}$, and $NEMO^{L227P}$ were performed using a Tycho NT.6 instrument (NanoTemper Technologies). In brief, the samples were loaded as duplicates and heated in glass capillaries. While heating, the thermal unfolding profiles by internal fluorescence at 330 nm and 350 nm were recorded. Data analysis, data smoothing, and calculation of derivatives were done using the internal evaluation features of the NT.6 instrument.

2.7. CD spectroscopy

Coiled coil character and construct stability were assessed by circular dichroism (CD) spectroscopy. CD data were collected on an Aviv 420 instrument using a 2 mm path length cuvette. NEMO samples were analyzed at 4.6 μM in buffer containing 20 mM potassium phosphate pH 7.8 and 150 mM NaF. CD spectra measurements were performed from 190 to 280 nm at 20 °C and the mean residue ellipticity was calculated from the raw signal. The degree of α-helical content was detected from the ratio of ellipticity at 222 nm to 208 nm. Thermal melting curves were obtained through variable temperature scans at fixed wavelength (222 nm) from 10 °C to 85 °C at a 2 °C/min ramp rate. The melting temperature (T_m) for each protein was estimated from the maximum of a plot of the first derivative of ellipticity against temperature. Helical content was estimated from the CD spectra using a method “β-structure” through the BeStSel server [39].

3. Results

3.1. NEMO behaves in solution as a large hydrodynamic particle

Previous attempts by the authors at determining the three-dimensional structure of full-length or nearly full-length human NEMO proteins have thus far not met with success. The full-length NEMO protein has not yielded crystals either alone or in complex with IKK2. Therefore, in support of our efforts to characterize the size and oligomerization state of NEMO in solution, we generated a simplistic schematic diagram of NEMO combining existing structural knowledge of its parts and secondary structure prediction algorithms [40]. Our schemcatic diagram contains an undefined N-terminal region composed of amino acids 1–48 and an enigmatic intervening domain (IVD) between residues 110–194, that is

predicted to be entirely α-helical, in addition to regions defined structurally in previous studies (Fig. 1A).

We engineered DNA expression plasmids encoding full-length as well as various fragments of NEMO and expressed each of them separately in *E. coli* as N-terminal poly-histidine fusion proteins. Some of these NEMO constructs were designed to begin and/or end within suspected CC domains. These include the $NEMO^{1–130}$, $NEMO^{1–210}$, and $NEMO^{1–280}$ protein fragments, where superscript numbering reflects amino acids of human NEMO. $NEMO^{1–365}$ is a curious case since the structure of the segment bracketed by the CC2 domain (ends at residue 337 in crystal structures) and Pro-rich region (begins at residue 375) is not known, but the Jpred 3 secondary structure prediction algorithm describes the whole of 259–360 as α-helical. The resulting recombinant proteins were purified to homogeneity by nickel affinity and size-exclusion chromatography (SEC) (Fig. 1B). When the apparent molecular weight (MW) of each recombinant NEMO protein was determined by analytical scale SEC using as calibration a standard set of globular enzymes, all were observed to elute as particles many times larger than that of any individual NEMO protein (Fig. 1C; Supplementary Fig. 1; Table 1). This behavior is reflected in the endogenous multisubunit IKK complex that also exhibits high MW by SEC [8,10]. As SEC provides a measure of hydrodynamicity of a particle, and not a true measure of protein MW, it is not clear from these analyses whether NEMO runs as a large oligomer, as an extremely elongated molecule, or some combination.

3.2. Full-length human NEMO is a dimer in solution

In order to determine the shape-independent MW of NEMO in solution, we employed size-exclusion chromatography coupled with multi-angle light scattering (SEC-MALS). Experiments performed at 60 and 6 μM protein concentrations revealed an average MW of 95.0 kDa, a value that was in close agreement with the calculated mass of 96.4 kDa for a NEMO homodimer (Fig. 2A). This value varies significantly from the observed MW of > 700 kDa estimated from the elution volume of NEMO by SEC alone. This discordance suggests that the shape of the NEMO dimer in solution is extremely elongated rendering it to appear as a globular hydrodynamic particle of significantly larger mass.

In order to obtain a second independent measure of its oligomerization state in solution, we next performed sedimentation velocity analytical ultracentrifugation (AUC) experiments on NEMO under conditions of protein concentration and buffer solution that were identical to that used in the SEC-MALS experiments. Data were analyzed by Sedfit [38]. The C(S) distribution of different NEMO species in solution was dominated by one peak (nearly 80% of total protein) with apparent MW (MW) of 96 kDa, which is once again suggestive of a NEMO homodimer (Fig. 2B). A major axis ratio of 31.4 for this particle indicates that the NEMO dimer is a highly elongated particle in solution. We also observed two minor species (roughly 10% each) with apparent MW of 217 kDa and 477 kDa, that are consistent with NEMO tetramers and octamers, respectively. Taken together, however, these SEC-MALS and AUC data strongly indicate that NEMO exists predominantly as an abnormally elongated homodimer in solution.

3.3. NEMO dimerization stability is affected by deletion of structured elements

We next analyzed several NEMO deletion proteins by SEC-MALS to determine their respective sizes in solution. These experiments were repeated multiple times and with different preparations at 60 and 6 μM protein concentrations. $NEMO^{1–110}$, $NEMO^{1–250}$, $NEMO^{250–365}$, and $NEMO^{111–250}$ yielded particles of 30, 69, 30, and 35 kDa, respectively (Fig. 3A–D). Each of these measurements agrees well with mass of dimeric forms (28, 62, 32, and 36 kDa, respectively). Interestingly, $NEMO^{1–365}$ appeared as a trimer and $NEMO^{1–130}$ exhibited significant amounts of high MW species in addition to a clear dimeric species (Fig. 3E,F). These results suggest that disruption of NEMO by deletion of parts from either end can drastically influence its propensity to associate into higher order oligomers. This idea was corroborated by two additional protein fragments, $NEMO^{1–210}$ and $NEMO^{1–280}$, which behave in solution as 377 and 140 kDa particles, respectively (Supplementary Fig. 2). Thus, it appears that disruption of NEMO within a particular structured element, rather than at borders of that element, hinders self-dimerization and leads to its stabilization through alternative modes of oligomerization. These observations point to a complex mode for NEMO dimerization in which multiple elements can interact but do so in a manner that is influenced strongly by their flanking regions. Alternatively, it is possible that when helical NEMO coiled coil elements are disrupted via premature deletion the resulting disorder leads to non-native homo-oligomerization, which could result in either constitutive activation or inhibition of IKK.

To test the folding stability of NEMO and NEMO deletion construct proteins, we performed nano differential scanning fluorimetry (nanoDSF) measurements. Under this approach kinetics of temperature-dependent protein unfolding can be rapidly monitored in solution by measuring protein intrinsic fluorescence intensity simultaneously at two different wavelengths, 330 and 350 nm. Changes in fluorescence intensity and shift of the fluorescence maximum as measured by inflection point analysis indicate protein unfolding at the apparent melting temperature (T_m). By this method we found $NEMO^{250–365}$ to be the most stable of all NEMO proteins tested (Fig 3G, Supplementary Table 1). This construct corresponds generally to CC2 (Fig. 1A). The slight increased thermal stability of this fragment relative to full-length NEMO suggests that either one or both flanking regions destabilize self-dimerization of CC2. $NEMO^{1–365}$, in particular, appears less stable than $NEMO^{250–365}$ suggesting that the IVD negatively affects the dimerization stability of CC2. $NEMO^{1–210}$ and $NEMO^{1–130}$ also display decreased thermal stability and we failed to detect a major folding transition for $NEMO^{1–250}$ and $NEMO^{1–110}$ by nanoDSF suggesting these are kinetically unstable segments.

In order to experimentally investigate the nature of the NEMO IVD, secondary structure of the $NEMO^{1–210}$ protein was analyzed in solution under equilibrium conditions by circular dichroism (CD) spectroscopy. This fragment was found to be even more α-helical and slightly more thermally stable than the full-length NEMO (Fig. 3H,I). The combined thermal stability data reveal several key properties regarding NEMO in solution. First, the NEMO IVD indeed appears to exhibit α-helical secondary structure as predicted, though it is kinetically unstable. Second, this portion promotes self-dimerization of NEMO while also serving to weaken the stability of dimerization through CC2. Finally, full-length NEMO

exhibits relatively low native thermal stability in solution with T_m ~ 47 °C. Therefore, it is possible that rapid association and dissociation of NEMO coiled coils could serve in part to explain the observed complex behavior of NEMO in solution.

3.4. Disease-linked NEMO point mutations affect its solution behavior

Consistent with a complicated functional mechanism for NEMO, the severity of symptoms in patients with EDA-ID and IP is highly variable and dependent upon which specific mutations are present in NEMO. Using the same approach as we employed for generating recombinant full-length and deletion NEMO proteins, we prepared ten variant NEMO proteins each containing a single amino acid point mutation: D113N (IP), R123W (IP), V146G (IP), L153R (EDA-ID), Q157P (EDA-ID), A162P (EDA-ID), R173G (EDA-ID), R173Q (EDA-ID), R175P (EDA-ID), and L227P (EDA-ID). Nine of these map to the IVD and the abbreviation for the disease associated with each of these mutations is given in parentheses after the mutation. Analysis via SEC-MALS revealed that the D113N and L153R variants are dimers at 60 and 6 μM concentration similar to NEMO of native sequence (Fig 4A,B; Table 2). Oddly, the R123W variant was observed at 130 kDa, which is smaller than a trimer but larger than a dimer (Fig 4C). Each of the proline variants, Q157P, A162P, R175P, and L227P, exhibited varying degrees of higher order oligomerization relative to the wild-type NEMO (Fig. 4D–G). Some of these, such as Q157P and L227P, could only be measured accurately at 6 μM and either could not be detected (Q157P) or formed extremely high MW species (L227P) at 60 μM concentration. Though less sensitive to the effects of concentration, the A162P variant was measured at 336 kDa at 60 μM and 194 kDa at 6 μM.

We then tested the folding stability of the disease-linked variant NEMO proteins by nanoDFS and found that the variants can be classified into two groups based on their thermal stability. The D113N, V146G, L153R, and R173Q variants each exhibit major unfolding transitions at temperatures higher than wild-type NEMO, whereas Q157P, A162P, R173G, and R175P exhibit numerous small transitions across a broad range of temperatures (Fig 4H, Supplementary Table 1). Interestingly, L227P demonstrated no unfolding transition whatsoever across the entire temperature range tested suggesting it is highly kinetically unstable. We measured the secondary structure of the L227P variant in solution by CD spectroscopy and found that it displays α-helical structure to a similar degree as wild-type NEMO (Fig. 4I). We note that the disease-linked variant NEMO proteins that display elevated MW in solution by SEC-MALS also fail to undergo the thermally induced ~47 °C structural transition characteristic of wild-type NEMO. It is possible that the inability of these variants to readily dissociate from one another in solution is linked to their association with diseases such as IP and EDA-ID.

3.5. Binding to NEMO and its effect on the propensity of IKK2 to oligomerize

In order to observe the solution behavior of NEMO within the context of a multisubunit IKK complex, we combined our NEMO proteins with purified full-length IKK2 subunit proteins generated by recombinant baculovirus infection of Sf9 insect cell suspension cultures [37]. As described previously, NEMO and IKK2 are known to associate through noncovalent interaction between the KBD in NEMO (residues 49–109 in human NEMO) and the NEMO

binding domain (NBD) of IKK2 (human IKK2 residues 705–743) (Figs. 1A and 5A,B). Prior to formation of NEMO:IKK2 complexes, we analyzed IKK2 subunit oligomerization in solution via SEC-MALS and sedimentation equilibrium AUC (Fig. 5C,D). Both approaches identified major peaks that correspond to homodimers, which agrees with previously reported X-ray crystal structures of nearly full-length IKK2 proteins [9–11]. We note that AUC also detects measurable amounts of higher order oligomers at multiples of the homodimer MW. Transient higher order oligomerization is a signature of IKK2 homodimers in solution [10].

As mentioned previously, multisubunit IKK complexes purified directly from activated HeLa cells behave as 700–900 kDa particles in solution when analyzed by SEC. In light of the observation that NEMO behaves as an aberrantly large particle by SEC, we employed SEC-MALS to determine the shape-independent MW of our NEMO:IKK2 complex preparations (Fig 5E). This revealed an apparent MW of 303 kDa, which is only slightly larger than what one would expect for a $NEMO_2$:$IKK2_2$ heterotetrameric complex (calculated MW = 280 kDa). We next analyzed the complex by AUC sedimentation velocity and observed the major peak at 262 kDa, which we interpret as corresponding to the $NEMO_2$:$IKK2_2$ heterotetramer (Fig. 5F). Interestingly, we also observe clear signals that correspond to the MW for $NEMO_4$:$IKK2_4$ (heterooctamer), $NEMO_6$:$IKK2_6$ (heterododecamer), and so forth. Thus, IKK2 homodimers display a similar propensity to assemble into higher order oligomers in solution [10]. However, the addition of NEMO to IKK2 appears to strengthen its self-association into higher order oligomeric assemblies.

3.6. Effects of NEMO truncation or mutation on multisubunit IKK complex formation

We next tested whether NEMO deletion variants assemble with IKK2. For this study, we were limited to only those variants that retained the N-terminal KBD, which is known to mediate a strong association with the C-terminal NBD of IKK2. We mixed purified recombinant IKK2 in excess with various NEMO deletion construct proteins and then analyzed the resultant complexes by SEC-MALS. Most of the mixtures yielded peaks that correspond to $IKK2_2$:$NEMO_2$ heterotetrameric complexes (Fig. 6A–E). Other than nonspecific extremely large aggregates that accompanied all NEMO protein preparations, only $NEMO^{1–365}$ of the deletion construct proteins tested assembled into complexes with IKK2 that were significantly larger than the heterotetramer. This reinforces what we observed when studying the $NEMO^{1–365}$ protein alone that deletion within the Pro-rich linker renders NEMO prone to self-association, perhaps by leaving CC2 uncapped and capable of interaction with additional NEMO protein monomers. Finally, these observations suggest that NEMO could serve to modulate the natural propensity of IKK2 dimers to form higher order oligomers in solution and therefore control activation of multisubunit IKK complexes.

Finally, we tested whether the EDA-ID disease-associated L227P NEMO variant protein would also associate with IKK2 similarly to the truncated NEMO variants. We combined $NEMO^{L227P}$ with IKK2 and analyzed the resultant mixture by SEC-MALS (Fig. 6F). Only a relatively small amount of the variant protein appeared to associate with IKK2 in a manner that could be analyzed and the size of the resultant complex was nearly twenty times the

calculated combined MW of NEMO and IKK2, suggesting that mutation to proline of NEMO at residue 227 strongly induces even higher order oligomerization of resultant NEMO:IKK2 complexes. It is possible that the activation of IKK2 protein kinase activity that results from such oligomerization is one basis for the disease pathology associated with this mutation in NEMO.

4. Discussion

The IKK complex plays critical roles as an integrator of diverse cellular signaling inputs and as an inducer of select response gene expression via regulation of transcription factor NF-κB. However, despite many years of intensive investigation, the precise molecular mechanisms by which inactive IKK complexes switch to become catalytically active remain poorly understood. That the process culminates with phosphorylation at two serine residues within the activation segments of catalytic IKK subunits (serines 177 and 181 in human IKK2; 176 and 180 in human IKK1) is clear [13]. The nature and source of this catalytic subunit phosphorylation as well as the necessary role of the accessory NEMO protein subunit are, at best, only somewhat well understood.

One major impediment to the study of IKK activation has been a lack of high resolution structural models of functional multisubunit complexes. Early characterization was limited to the observation that active IKK that was either purified as an endogenous complex from HeLa cells or reconstituted through co-expression of individual subunits in insect cells appeared as a high MW particle within the range of 700–900 kDa [6–8]. This high MW form of IKK was associated with its activated state until it was firmly established that both inactive and active forms of IKK appear as similarly large particles in SEC and that IKK activation via activation segment phosphorylation was not associated with significant changes in size of the complex [10]. Detailed X-ray crystallographic analyses of nearly full-length IKK2 proteins revealed that they form well-folded homodimers with a propensity to self-associate as higher order oligomers [9–11]. Critical questions that remain concern the nature and structure of the multisubunit IKK complex and the mechanism by which it is able to become activated in response to diverse cellular stress signals.

To address these questions and in the absence of any structure for full-length NEMO, we focused our attention on its behavior in solution. In light of the relatively well-folded structures of the catalytic subunit dimers, we assumed NEMO to be responsible for the observed large particle size of IKK in solution. This is consistent with original observations that in cells devoid of NEMO, IKK catalytic subunits were purified as roughly 300 kDa complexes [41]. Three major parts of NEMO, the KBD, CC1, and CC2, that have been studied by X-ray crystallography all appear as imperfect homodimeric coiled coils [24–30]. In order to improve understanding of the structure of full-length NEMO and its influence on multisubunit IKK complex in solution, we have carried out biophysical characterization via SEC, SEC-MALS, AUC, nanoDFS, and CD spectroscopy on purified full-length NEMO and a series of NEMO deletion constructs and variants containing disease-linked point mutations as well as various NEMO:IKK2 complexes.

Our SEC-MALS and AUC sedimentation velocity experiments firmly establish that NEMO preferentially forms homodimers of ~100 kDa in solution. When one considers that the same full-length NEMO homodimers elute from analytical SEC at the same volume as globular proteins of > 700 kDa, it seems clear that NEMO dimers do not exhibit a compact fold. This conclusion is further corroborated by our sedimentation velocity analysis of NEMO in solution that fits the ratio of the major axes of NEMO at > 30. SEC-MALS analysis of NEMO deletion constructs revealed that they also form homodimers in solution, with the important caveat that when deletions are within defined structural elements that flank CC1 and CC2, aberrantly large and/or mixtures of higher MW oligomers were detected. We note that previous attempts at small-angle x-ray scattering (SAXS) measurements on NEMO and NEMO:IKK2 complexes failed to yield interpretable data, likely on account of low concentration of the former sample and heterogeneous oligomerization for the latter. In light of our improved ability to analyze multisubunit IKK complexes in solution by immediate light scattering of SEC purified samples, we look forward to pursuing SEC-SAXS studies as well as negative stain transmission electron microscopy of SEC purified IKK proteins and complexes. Taken together, these observations lead us to conclude that rather than assembling as one long homodimer through the additive influence of three separate coiled coil regions in a long array, the NEMO homodimer is held together through a mutually regulatory dynamic association/competition between individual elements. On the basis of our observations, we hypothesize that NEMO residues 110–250, comprising the IVD and CC1, plays a critical role in this process by modulating the association of the flanking coiled coil CC2 element (Fig 7). The manner by which the IVD-CC1 region might accomplish this is not clear. However, in light of structural prediction and CD data that strongly support α-helical secondary structure for this segment as well as the increased thermal stability we observe for deletion proteins that contain the central region, we propose that the IVD exerts control over NEMO dimerization through flanking coiled coil regions, perhaps by competitively adopting its own unique helical homodimeric structure. In support of such a model, we note that many point mutations within this region are associated with disease phenotypes and our analysis of several of these variant NEMO proteins revealed that they exhibit drastically altered solution behavior.

Analysis of assembled NEMO:IKK2 complexes in solution both by SEC-MALS and AUC clearly reveals that although its predominant state is a $NEMO_2$:$IKK2_2$ tetramer, it can also form higher order $(NEMO_2:IKK_2)_n$ oligomers. It is interesting that C-terminal deletions to NEMO do not appear to influence the ability of the multisubunit IKK heterotetramer to assemble so long as the KBD is preserved in NEMO. This might suggest that association of dynamic NEMO to IKK2 dimers serves to attenuate whatever influence the IVD exerts on NEMO structure and dynamics. Of even more interest, however, is that the combination of NEMO with IKK2 does not appear to alter the solution oligomerization states for either of the separate proteins—both NEMO and IKK2 remain as homodimers In the absence of additional knowledge concerning the surfaces employed by IKK2 and, to a lesser degree, NEMO homodimers to induce oligomerization of multisubunit IKK, it is challenging to predict how NEMO exerts control over higher order oligomerization of IKK. It remains to be determined what, if any, functional significance is owed to higher order oligomerization of $NEMO_2$:$IKK2_2$ tetramers in the cell.

The significance of the observed structural plasticity of NEMO is evident from the involvement of various altered forms of the protein in disease. As mentioned previously, NEMO is frequently mutated in two human disorders: Anhidrotic Ectodermal Dysplasia with Immunodeficiency (EDA-ID) and Incontinentia Pigmenti (IP). Male EDA-ID patients with hemizygous NEMO mutations retain residual NF-κB activation (hypomorphic mutations), whereas in female patients the NEMO mutation is always heterozygous resulting either in maintenance of residual NF-κB activation (EDA-ID) or its near abolition (IP) [19,42,43], or in some cases constitutive activation of IKK2 [44]. This suggests that specific mutations impact the control of IKK over NF-κB from particular signaling inputs [45]. This further reinforces the idea that NEMO responds to different signals in distinct manners which can be accomplished by modulation over the structural plasticity of NEMO by its modular coiled coil regions, many of which are capable of dimerization and association with other factors. We note that similar conclusions were drawn from a study that employed solution biophysical methods to observe changes in NEMO structure as a consequence of binding to linear ubiquitin and identification of the IVD as a regulatory element in NEMO was proposed recently in published study by Shaffer, et al. [46,47]. Our observation that many disease-causing NEMO variant proteins display altered oligomerization states in solution reinforces the idea that NEMO exerts its control over IKK activation by integrating diverse cellular signals to regulate higher order oligomerization of IKK complexes.

Supplementary Material

Refer to Web version on PubMed Central for supplementary material.

Acknowledgements

The authors thank B. Maniaci, V. Upadhye, and J.J. Love for help with SEC-MALS and CD instrumentation and data collection. We thank S. Howell for use of the NanoTemper instrument and P. Jennings for helpful discussion. This research was supported by grants from NIH (CA141722), the University of California Tobacco-Related Disease Research Program (TRDRP), and American Association for Cancer Research (AACR) to GG and NIH (CA197999) to TH. Biochemistry research at SDSU is supported in part by the California Metabolic Research Foundation.

Abbreviations:

AUC	Analytical ultracentrifugtation
CC	Coiled coil
CD	Circular dichroism
EDA-ID	Ectodermal dysplasia anhidrotic with immunodeficiency
IP	Incontinentia pigmenti
IKK	IκB Kinase
IVD	Intervening domain
KBD	Kinase binding domain

KD	Kinase domain
MALS	Multi-angle light scattering
T_m	Melting temperature
MW	Molecular weight
nanoDSF	Nano differential scanning fluorimetry
NBD	NEMO binding domain
NEMO	NF-κB essential modulator
SAXS	Small-angle x-ray scattering
SDD	Scaffold dimerization domain
SEC	Size-exclusion chromatography
ULD	Ubiquitin-like domain
ZF	Zinc finger

References

[1]. Hayden MS, Ghosh S, Shared principles in NF-κB signaling, Cell 132 (2008) 344–362. [PubMed: 18267068]

[2]. Mulero MC, Huxford T, Ghosh G, NF-κB, IκB, and IKK: integral components of immune system signaling, Adv. Exp. Med. Biol 1172 (2019) 207–226. [PubMed: 31628658]

[3]. Scheidereit C, IκB kinase complexes: gateways to NF-κB activation and transcription, Oncogene 25 (2006) 6685–6705. [PubMed: 17072322]

[4]. Huxford T, Ghosh G, A structural guide to proteins of the NF-κB signaling module, Cold Spring Harb. Perspect. Biol 1 (2009) a000075. [PubMed: 20066103]

[5]. Chen ZJ, Parent L, Maniatis T, Site-specific phosphorylation of IκBα by a novel ubiquitination-dependent protein kinase activity, Cell 84 (1996) 853–862. [PubMed: 8601309]

[6]. DiDonato JA, Hayakawa M, Rothwarf DM, Zandi E, Karin M, A cytokine-responsive IκB kinase that activates the transcription factor NF-κB, Nature 388 (1997) 548–554. [PubMed: 9252186]

[7]. Mercurio F, Zhu H, Murray BW, Shevchenko A, Bennett BL, Li J, Young DB, Barbosa M, Mann M, Manning A, Rao A, IKK-1 and IKK-2: cytokine-activated IκB kinases essential for NF-κB activation, Science 278 (1997) 860 866. [PubMed: 9346484]

[8]. Zandi E, Rothwarf DM, Delhase M, Hayakawa M, Karin M, The IκB kinase complex (IKK) contains two kinase subunits, IKKα and IKKβ, necessary for IκB phosphorylation and NF-κB activation, Cell 91 (1997) 243–252. [PubMed: 9346241]

[9]. Xu G, Lo YC, Li Q, Napolitano G, Wu X, Jiang X, Dreano M, Karin M, Wu H, Crystal structure of inhibitor of κB kinase β, Nature 472 (2011) 325–330. [PubMed: 21423167]

[10]. Polley S, Huang DB, Hauenstein AV, Fusco AJ, Zhong X, Vu D, Schröfelbauer B, Kim Y, Hoffmann A, Verma IM, Ghosh G, Huxford T, A structural basis for IκB kinase 2 activation via oligomerization-dependent *trans* auto-phosphorylation, PLoS Biol 11 (2013) e1001581. [PubMed: 23776406]

[11]. Liu S, Misquitta YR, Olland A, Johnson MA, Kelleher KS, Kriz R, Lin LL, Stahl M, Mosyak L, Crystal structure of a human IκB kinase β asymmetric dimer, J. Biol. Chem 288 (2013) 22758–22767. [PubMed: 23792959]

[12]. Hauenstein AV, Rogers WE, Shaul JD, Huang DB, Ghosh G, Huxford T, Probing kinase activation and substrate specificity with an engineered monomeric IKK2, Biochemistry 53 (2014) 2064–2073. [PubMed: 24611898]

[13]. Delhase M, Hayakawa M, Chen Y, Karin M, Positive and negative regulation of IκB kinase activity through IKKβ subunit phosphorylation, Science 284 (1999) 309–313. [PubMed: 10195894]

[14]. Nolen B, Taylor S, Ghosh G, Regulation of protein kinases; controlling activity through activation segment conformation, Mol. Cell 15 (2004) 661–675. [PubMed: 15350212]

[15]. Polley S, Passos DO, Huang DB, Mulero MC, Mazumder A, Biswas T, Verma IM, Lyumkis D, Ghosh G, Structural basis for the activation of IKKI/α, Cell Rep 17 (2016) 1907–1914. [PubMed: 27851956]

[16]. Senftleben U, Cao Y, Xiao G, Greten FR, Krahn G, Bonizzi G, Chen Y, Hu Y, Fong A, Sun SC, Karin M, Activation by IKKα of a second, evolutionary conserved, NF-κB signaling pathway, Science 293 (2001) 1495–1499. [PubMed: 11520989]

[17]. Xiao G, Harhaj EW, Sun SC, NF-κB-inducing kinase regulates the processing of NF-κB2 p100, Mol. Cell 7 (2001) 401–409. [PubMed: 11239468]

[18]. Rudolph D, Yeh WC, Wakeham A, Rudolph B, Nallainathan D, Potter J, Elia AJ, Mak TW, Severe liver degeneration and lack of NF-κB activation in NEMO/IKKγ-deficient mice, Genes Dev 14 (2000) 854–862. [PubMed: 10766741]

[19]. Schmidt-Supprian M, Bloch W, Courtois G, Addicks K, Israël A, Rajewsky K, Pasparakis M, NEMO/IKK gamma-deficient mice model incontinentia pigmenti, Mol. Cell 5 (2000) 981–992. [PubMed: 10911992]

[20]. Chen J, Chen ZJ, Regulation of NF-κB by ubiquitination, Curr. Opin. Immunol 25 (2013) 4–12. [PubMed: 23312890]

[21]. Rothwarf DM, Zandi E, Natoli G, Karin M, IKKγ is an essential regulatory subunit of the IκB kinase complex, Nature 395 (1998) 297–300. [PubMed: 9751060]

[22]. May MJ, D'Acquisto F, Madge LA, Glockner J, Pober JS, Ghosh S, Selective inhibition of NF-κB activation by a peptide that blocks the interaction of NEMO with the IκB kinase complex, Science 289 (2000) 1550–1554. [PubMed: 10968790]

[23]. May MJ, Marienfeld RB, Ghosh S, Characterization of the κB-kinase NEMO binding domain, J. Biol. Chem 277 (2002) 45992–46000. [PubMed: 12244103]

[24]. Barczewski AH, Ragusa MJ, Mierke DF, Pellegrini M, The IKK-binding domain of NEMO is an irregular coiled coil with a dynamic binding interface, Sci. Rep 9 (2019) 2950. [PubMed: 30814588]

[25]. Rushe M, Silvian L, Bixler S, Chen LL, Cheung A, Bowes S, Cuervo H, Berkowitz S, Zheng T, Guckian K, Pellegrini M, Lugovskoy A, Structure of a NEMO/IKK-associating domain reveals architecture of the interaction site, Structure 16 (2008) 798–808. [PubMed: 18462684]

[26]. Bagnéris C, Ageichik AV, Cronin N, Wallace B, Collins M, Boshoff C, Waksman G, Barrett T, Crystal structure of a vFlip-IKKγ complex: insights into viral activation of the IKK signalosome, Mol. Cell 30 (2008) 620–631. [PubMed: 18538660]

[27]. Rahighi S, Ikeda F, Kawasaki M, Akutsu M, Suzuki N, Kato R, Kensche T, Uejima T, Bloor S, Komander D, Randow F, Wakatsuki S, Dikic I, Specific recognition of linear ubiquitin chains by NEMO is important for NF-κB activation, Cell 136 (2009) 1098–1109. [PubMed: 19303852]

[28]. Lo YC, Lin SC, Rospigliosi CC, Conze DB, Wu CJ, Ashwell JD, Eliezer D, Wu H, Structural basis for recognition of diubiquitins by NEMO, Mol. Cell 33 (2009) 602–615. [PubMed: 19185524]

[29]. Yoshikawa A, Sato Y, Yamashita M, Mimura H, Yamagata A, Fukai S, Crystal structure of the NEMO ubiquitin-binding domain in complex with Lys 63-linked diubiquitin, FEBS Lett 583 (2009) 3317–3322. [PubMed: 19766637]

[30]. Fujita H, Rahighi S, Akita M, Kato R, Sasaki Y, Wakatsuki S, Iwai K, Mechanism underlying IκB kinase activation mediated by the linear ubiquitin chain assembly complex, Mol. Cell. Biol 34 (2014) 1322–1335. [PubMed: 24469399]

[31]. Saito K, Kigawa T, Koshiba S, Sato K, Matsuo Y, Sakamoto A, Takagi T, Shirouzu M, Yabuki T, Nunokawa E, Seki E, Matsuda T, Aoki M, Miyata Y, Hirakawa N, Inoue M, Terada T, Nagase T,

Kikuno R, Nakayama M, Ohara O, Tanaka A, Yokoyama S, The CAP-Gly domain of CYLD associates with the proline-rich sequence in NEMO/IKKγ, Structure 12 (2004) 1719–1728. [PubMed: 15341735]

[32]. Cordier F, Grubisha O, Traincard F, Veron M, Delepierre M, Agou F, The zinc finger of NEMO is a functional ubiquitin-binding domain, J. Biol. Chem 284 (2009) 2902–2907. [PubMed: 19033441]

[33]. Smahi A, Courtois G, Rabia SH, Döffinger R, Bodemer C, Munnich A, Casanova JL, Israël A, The NF-κB signalling pathway in human diseases: from incontinentia pigmenti to ectodermal dysplasias and immune-deficiency syndromes, Hum. Mol. Genet 11 (2002) 2371–2375. [PubMed: 12351572]

[34]. Agou F, Ye F, Goffinont S, Courtois G, Yamaoka S, Israël A, Veron M, NEMO trimerizes through its coiled-coil C-terminal domain, J. Biol. Chem 277 (2002) 17464–17475. [PubMed: 11877453]

[35]. Drew D, Shimada E, Huynh K, Bergqvist S, Talwar R, Karin M, Ghosh G, Inhibitor κB kinase β binding by inhibitor κB kinase γ, Biochemistry 46 (2007) 12482–12490. [PubMed: 17924664]

[36]. Tegethoff S, Behlke J, Scheidereit C, Tetrameric oligomerization of IκB kinase γ (IKKγ) is obligatory for IKK complex activity and NF-κB activation, Mol. Cell. Biol 23 (2003) 2029–2041. [PubMed: 12612076]

[37]. Shaul JD, Farina A, Huxford T, The human IKKβ subunit kinase domain displays CK2-like phosphorylation specificity, Biochem. Biophys. Res. Commun 374 (2008) 592–597. [PubMed: 18657515]

[38]. Chaturvedi SK, Ma J, Brown PH, Zhao H, Schuck P, Measuring macromolecular size distributions and interactions at high concentrations by sedimentation velocity, Nat. Commun 9 (2018) 4415. [PubMed: 30356043]

[39]. Micsonai A, Wien F, Kernya L, Lee YH, Goto Y, Refregiers M, Kardos J, Accurate secondary structure prediction and fold recognition for circular dichroism spectroscopy, Proc. Natl. Acad. Sci. U. S. A 112 (2015) E3095–E3103. [PubMed: 26038575]

[40]. Cole C, Barber JD, Barton GJ, The Jpred 3 secondary structure prediction server, Nucleic Acids Res 36 (2008) W197–W201. [PubMed: 18463136]

[41]. Yamaoka S, Courtois G, Bessia C, Whiteside ST, Weil R, Agou F, Kirk HE, Kay RJ, Israël A, Complementation cloning of NEMO, a component of the IκB kinase complex essential for NF-κB activation, Cell 93 (1998) 1231–1240. [PubMed: 9657155]

[42]. Smahi A, Courtois G, Vabres P, Yamaoka S, Heuertz S, Munnich A, Israël A, Heiss NS, Klauck SM, Kioschis P, Wiemann S, Poustka A, Esposito T, Bardaro T, Gianfrancesco F, Ciccodicola A, D'Urso M, Woffendin H, Jakins T, Donnai D, Stewart H, Kenwrick SJ, Aradhya S, Yamagata T, Levy M, Lews RA, Nelson DL, Genomic rearrangement in NEMO impairs NF-κB activation and is a cause of incontinentia pigmenti. The international Incontinentia Pigmenti (IP) consortium, Nature 405 (2000) 466–472. [PubMed: 10839543]

[43]. Döffinger R, Smahi A, Bessia C, Geissmann F, Feinberg J, Durandy A, Bodemer C, Kenwrick S, Dupuis-Girod S, Blanche S, Wood P, Rabia SH, Headon DJ, Overbeek PA, Le Deist F, Holland SM, Belani K, Kumararatne DS, Fischer A, Shapiro R, Conley ME, Reimund E, Kalhoff H, Abinun M, Munnich A, Israël A, Courtois G, Casanova JL, X-linked anhidrotic ectodermal dysplasia with immunodeficiency is caused by impaired NF-κB signaling, Nat. Genet 27 (2001) 277–285. [PubMed: 11242109]

[44]. Zilberman-Rudenko J, Shawver LM, Wessel AW, Luo Y, Pelletier M, Tsai WL, Lee Y, Vonortas S, Cheng L, Ashwell JD, Orange JS, Siegel RM, Hanson EP, Recruitment of A20 by the C-terminal domain of NEMO suppresses NF-κB activation and autoinflammatory disease, Proc. Natl. Acad. Sci. U. S. A 113 (2016) 1612–1617. [PubMed: 26802121]

[45]. Fusco F, Pescatore A, Conte MI, Mirabelli P, Paciolla M, Esposito E, Lioi MB, Ursini MV, EDA-ID and IP, two faces of the same coin: how the same IKBKG/NEMO mutation affecting the NF-κB pathway can cause immunodeficiency and/or inflammation, Int. Rev. Immunol 34 (2015) 445–459. [PubMed: 26269396]

[46]. Hauenstein AV, Xu G, Kabaleeswaran V, Wu H, Evidence for M1-linked polyubiquitin-mediated conformational change in NEMO, J. Mol. Biol 429 (2017) 3793–3800. [PubMed: 29111346]

[47]. Shaffer R, DeMaria AM, Kagermazova L, Liu Y, Babaei M, Caban-Penix S, Cervantes A, Jehle S, Makowski L, Gilmore TD, Whitty A, Allen KN, A central region of NF-κB essential modulator is required for IKKβ-induced conformational change and for signal propagation, Biochemistry 58 (2019) 2906–2920. [PubMed: 31145594]

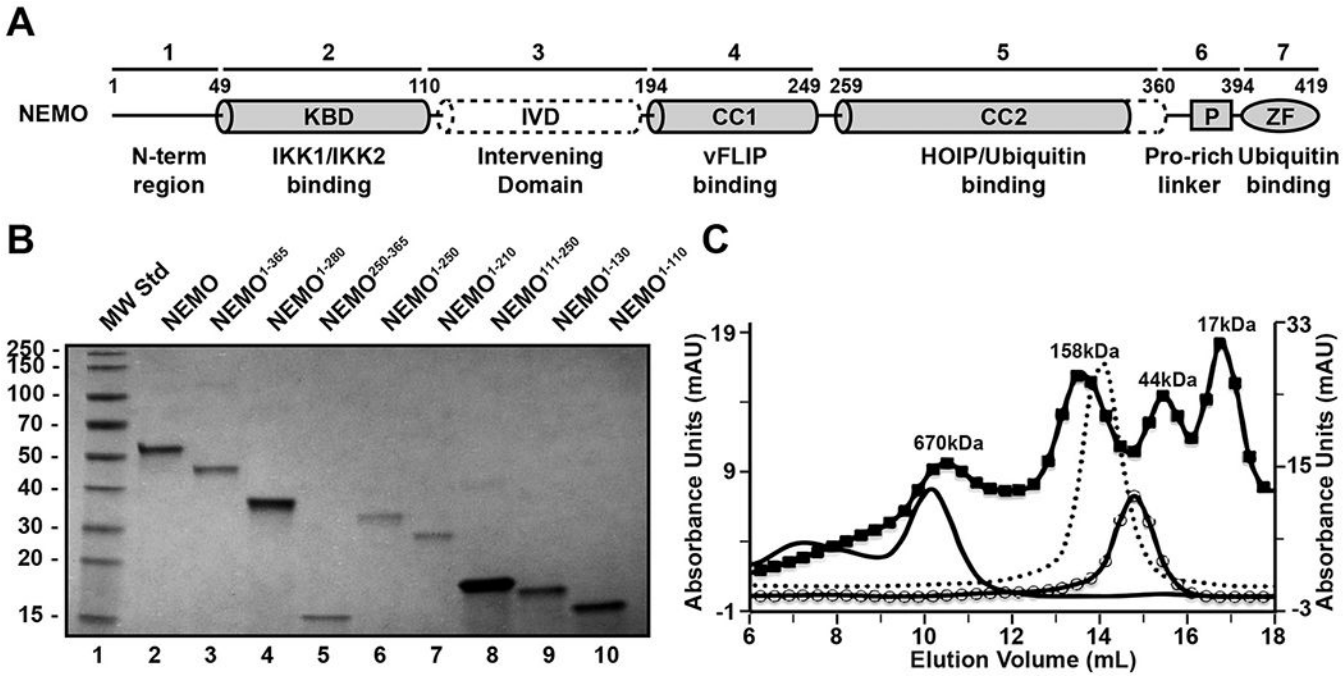

Fig. 1.

Recombinant full-length human NEMO protein and deletion constructs. A) Two-dimensional structural diagram of human NEMO protein. Portions of known structure are shaded grey and known or suspected helical regions are depicted as cylinders. The linear structure is divided into seven segments (numbered above): 1-An amino-terminal segment; 2-the kinase binding domain (KBD) that interacts through noncovalent association with the C-terminal NEMO-binding domain (NBD) of either IKK1 or IKK2; 3) an enigmatic intervening domain (IVD) that is predicted to be helical (dashed cylinder); 4) the first of two colied coil regions (CC1) that has been shown to interact with viral protein vFLIP; 5) a second coiled-coil (CC2) that associates with the HOIP protein of the LUBAC complex and linear ubiquitin; 6) a linker that ends in a Pro-rich sequence; 7) a zinc finger motif that has been shown to interact with ubiquitin. Approximate amino acid numbering (1–419) is given at each segment border. B) Coomassie-stained SDS-PAGE analysis of recombinant full-length (lane 2) and deletion construct human NEMO proteins (lanes 3–10). C) Analytical SEC chromatograms of full-length NEMO (solid line) and NEMO deletion constructs $NEMO^{250–365}$ (dotted line) and $NEMO^{1–110}$ (solid line with hollow circles) overlaid on calibration standard (solid line with filled squares) with known MW of standard proteins labeled in kilodaltons (kDa).

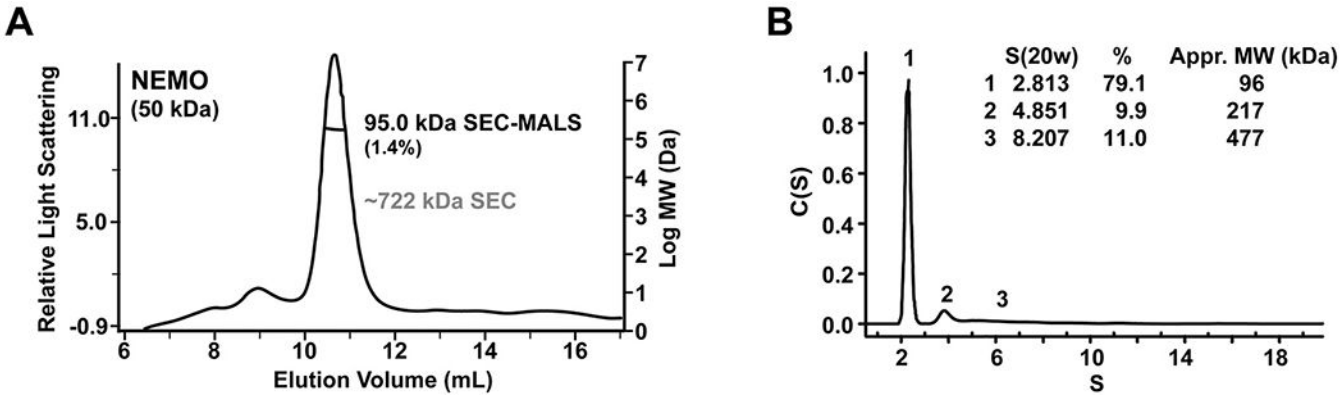

Fig. 2.

Shape-independent size determination of full-length human NEMO in solution. A) Size-exclusion chromatography with multi-angle light scattering (SEC-MALS) analysis of 6 μM sample. The calculated MW of the His-tagged monomer is 50 kDa. Determined MW is given in kilodaltons (kDa) with percent error in measurement. The apparent MW determined previously by SEC only is given in grey. B) Analytical ultracentrifugation (AUC) sedimentation velocity measurement data for full-length NEMO. Peaks are assigned to a percentage value (fraction of total protein detected) and approximate MW.

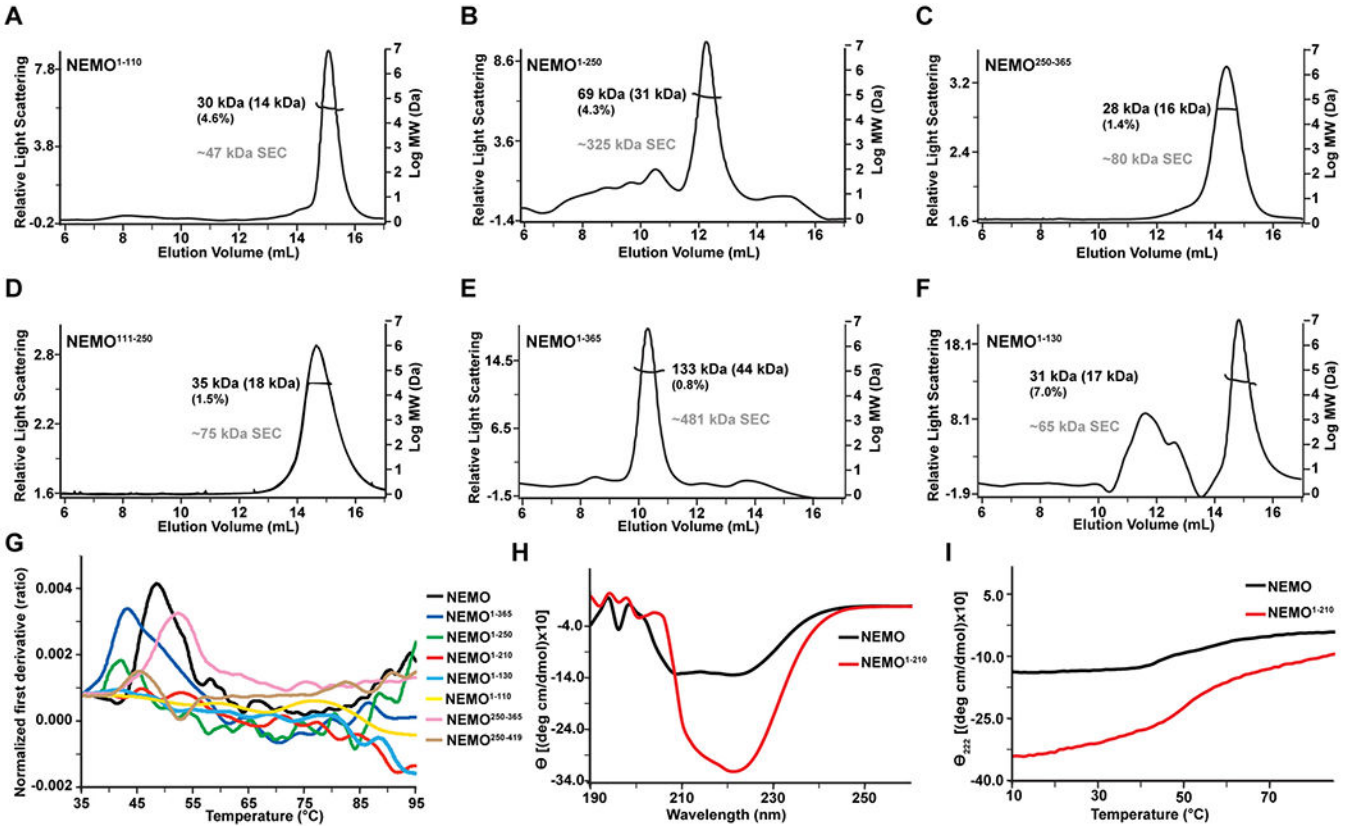

Fig. 3.

Analysis of NEMO deletion constucts in solution. A) SEC-MALS analysis of NEMO$^{1–110}$. For all NEMO deletion construct SEC-MALS chromatograms, monomer MW is given in parentheses above the percent error. Apparent MW determined by SEC only is in grey. B) SEC-MALS analysis of NEMO$^{1–250}$, C) NEMO$^{250–365}$, D) NEMO$^{111–250}$, E) NEMO$^{1–365}$, and F) NEMO$^{1–130}$. G) NanoDFS analysis of deletion construct NEMO proteins. Each colored line represents measurement of the NEMO protein construct indicated. H) Circular dichroism (CD) spectroscopy of full-length NEMO (black line) and NEMO$^{1–210}$ (red line). I) Temperature-dependent CD signal at 222 nm of full-length NEMO (black) and NEMO$^{1–210}$ (red).

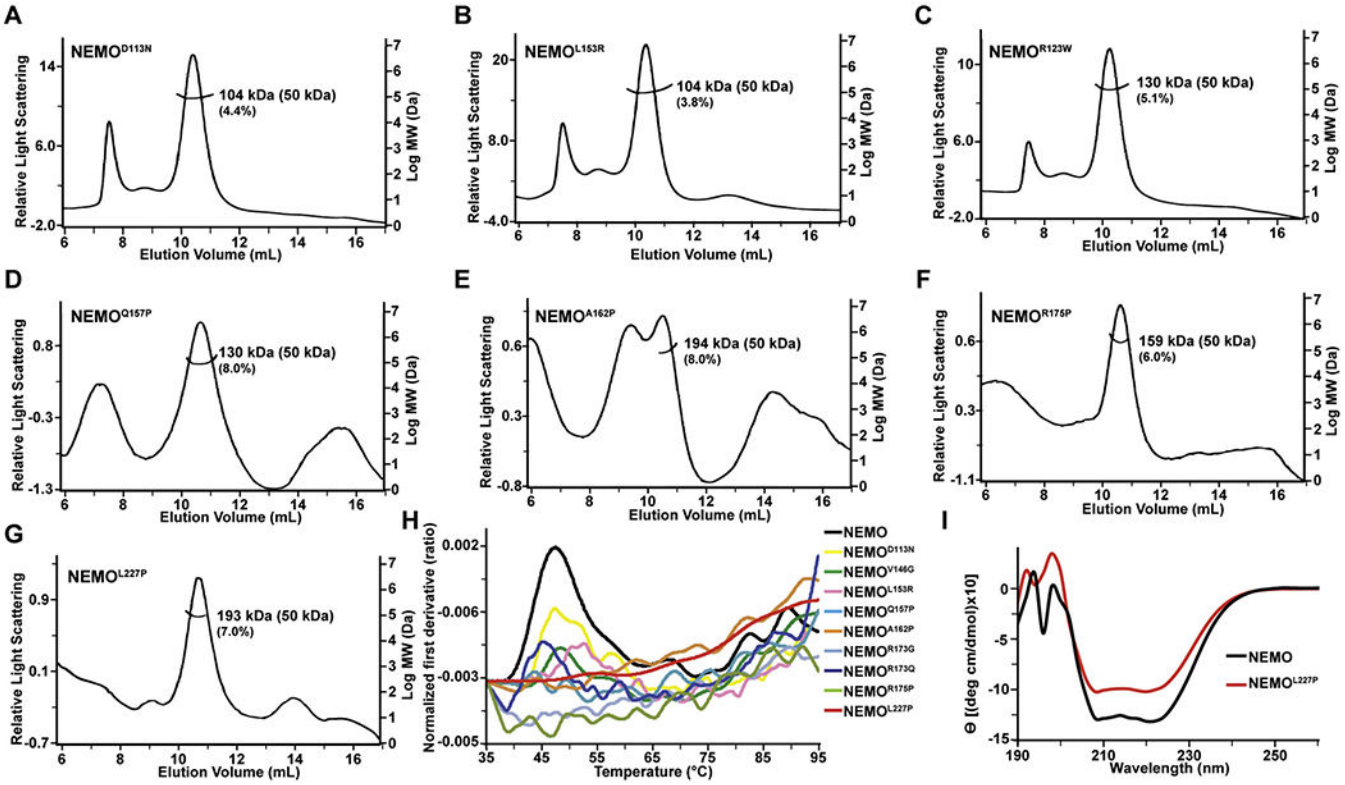

Fig. 4.

Analysis of variant NEMO proteins containing disease-linked point mutations in solution. A) SEC-MALS analysis of NEMO^{D113N}, B) NEMO^{L153R}, C) NEMO^{R123W}, D) NEMO^{Q157P}, E) NEMO^{A162P}, F) NEMO^{R175P}, and G) NEMO^{L227P} each at 6 μM concentration. H) NanoDFS analysis of disease-linked NEMO variants. Each colored line represents measurement of the NEMO variant protein indicated. I) CD spectroscopy of full-length wild-type NEMO (black line) and NEMO^{L227P} (red line).

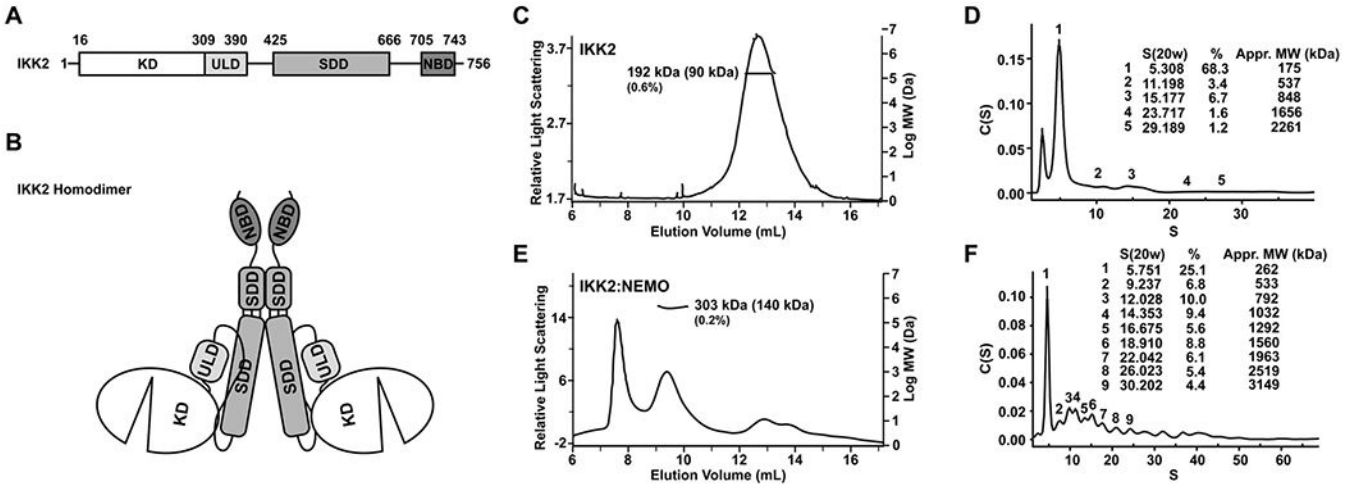

Fig. 5.

Solution analysis of recombinant full-length IKK2 protein and NEMO:IKK2 complex. A) Domain organization of the IKK2 subunit with kinase domain (KD), ubiquitin-like domain (ULD), and scaffold-dimerization domain (SDD) labeled and human amino acid numbering indicated. B) Schematic representation of the IKK2 homodimer depicting the relative arrangement of domains and homodimerization through the portion of the SDD distal to the KD and ULD. C) SEC-MALS chromatogram of full-length human IKK2 protein. D) AUC sedimentation velocity measurement of full-length human IKK2 in solution. E) SEC-MALS chromatogram of recombinant IKK2:NEMO complex. F) AUC sedimentation velocity measurement of the IKK2:NEMO complex.

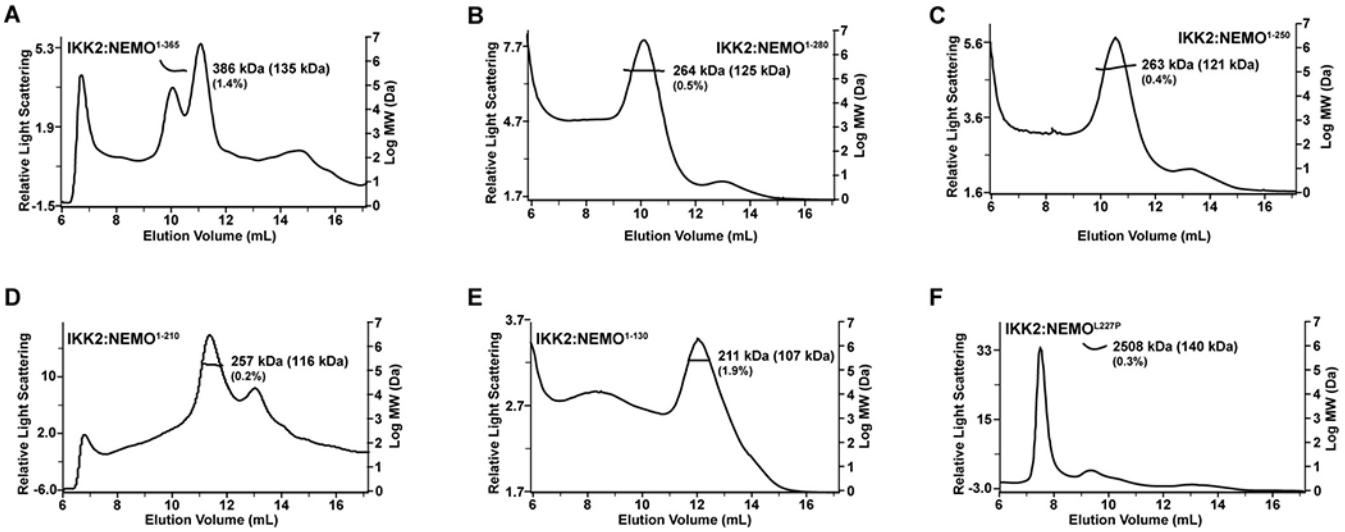

Fig. 6.

Solution analysis of IKK2 in complex with NEMO protein variants. SEC-MALS chromatograms of full-length human IKK2 protein in complex with A) $NEMO^{1–365}$, B) $NEMO^{1–280}$, C) $NEMO^{1–250}$, D) $NEMO^{1–210}$, E) $NEMO^{1–130}$, and F) $NEMO^{L227P}$.

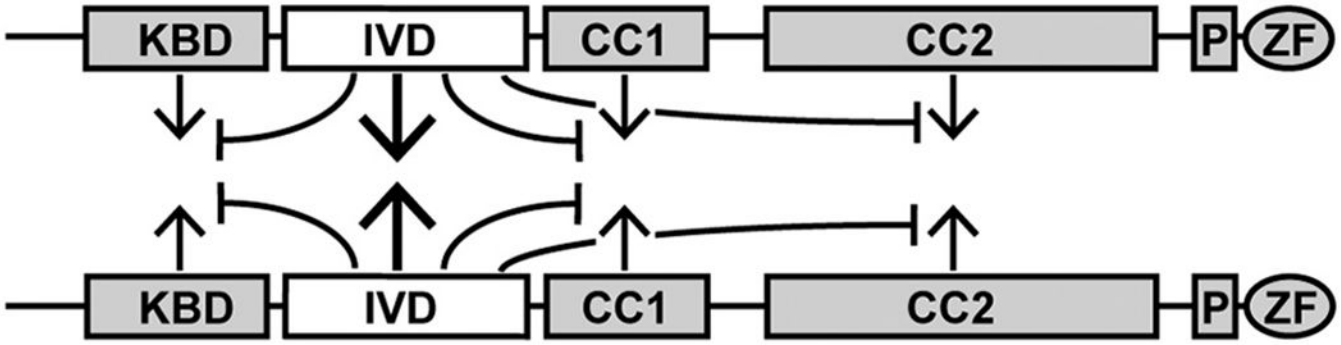

Fig. 7.

Schematic of the proposed role of NEMO IVD in influencing dimerization of flanking coiled coil regions of NEMO, which either on their own or through association with additional factors are capable of dimerization. Abbreviations for individual NEMO structural elements are the same as in Fig. 1A and those elements of known structure are shaded grey.

Table 1

Apparent molecular weight of human NEMO and NEMO deletion proteins by size exclusion chromatography.

Protein	MW of monomer (kDa)	Elution vol. (mL)	Apparent MW (kDa)
NEMO	50.2	10.39	721.9
$NEMO^{1–365}$	44.4	10.90	481.4
$NEMO^{1–280}$	34.6	11.98	353.2
$NEMO^{1–250}$	31.2	12.15	325.0
$NEMO^{1–210}$	26.3	12.93	217.9
$NEMO^{1–130}$	17.4	15.01	65.3
$NEMO^{1–110}$	14.9	15.54	46.5
$NEMO^{111–250}$	18.5	14.78	75.4
$NEMO^{250–365}$	13.8	14.68	80.2

Table 2

Molecular weight of full length human NEMO proteins measured in solution by SEC-MALS*.

NEMO variant	MW in kDa (% error)
Wild type	95.0 (1.4)
D113N	104.4 (4.4)
R123W	129.7 (5.1)
L153R	104.0 (3.8)
Q157P (6 μM)	130.4 (8.0)
A162P	336.1 (4.0)
A162P (6 μM)	194.0 (8.0)
R175P	159.2 (2.8)
L227P (6 μM)	193.0 (7.0)

* Measured at 60 μM protein concentration unless indicated.